THE EFFECT OF VISCOELASTIC BRAIN ON THE DYNAMIC CHARACTERISTICS OF THE HUMAN SKULL - BRAIN SYSTEM

A. Charalambopoulos, D.I. Fotiadis, A. Ktena and C.V. Massalas

14-97

Preprint no. 14-97/1997

Department of Computer Science
University of Ioannina
451 10 Ioannina, Greece

THE EFFECT OF VISCOELASTIC BRAIN ON THE DYNAMIC CHARACTERISTICS OF THE HUMAN SKULL - BRAIN SYSTEM

A. CHARALAMBOPOULOS

Institute of Chemical Engineering and High Temperature Chemical Processes, GR 265 00 Patras, Greece

D.I. FOTIADIS, A. KTENA

Dept. of Computer Science, University of Ioannina, GR 451 10 Ioannina Greece

and

C.V. MASSALAS*

Dept. of Mathematics, University of Ioannina, GR 451 10 Ioannina, Greece

Key Words: Free Vibrations, Head - Neck System, Cranial Biomechanics.

Abstract

In this paper, we present a solution to the problem of free vibrations of the human head system taking into account the dissipative behaviour of the brain. The mathematical model is based on the three - dimensional theory of viscoelasticity and the representation of the displacement field in terms of the Navier eigenvectors. The frequency equation is solved numerically and the results for eigenfrequencies and damping coefficients are presented for various geometrical and physical parameters of the system. The results obtained are in excellent agreement with the measured eigenfrequencies and the predicted damping coefficients are within the order of magnitude of the measured ones. From the proposed analysis we have obtained the information that the role of the viscoelastic neck as well as the viscoelastic properties of the skull - brain system have to be simultaneously taken into account in the study of the frequency spectrum of the human head. The analysis of the realistic model is under preparation.

* Author to whom correspondence should be addressed

1. Introduction

One of the most important branches of biomechanics concerns the field of head injuries because a high percentage of accidents, leading to fatalities, involve harm of the head, which constitutes the most vulnerable part of the human body. The necessity of confronting all the consequences of such accidents and recovering totally the brain functions has augmented rapidly the application field of cranial biomechanics together with the corresponding theoretical and experimental knowledge.

There are two main approaches towards the study of head properties and characteristics involving the injury procedure: The physical approach, which is based on experimental analysis and the mathematical one that exploits the possibility of simulation of the geometric and physical characteristics of the human head with simplified structures-in shape and substance. The mathematical modelling of the brain system has drawn the attention of many researchers in recent years [1-3]. One of the most important topics in the framework of study of the head system is the determination of the relation between the dynamical characteristics of the human head with the perturbed physical parameters due to injury. There exist a lot of models simulating the whole head system and its dynamical characteristics, each one of which makes some simplifications as far as geometric and/or physical properties are concerned. However, almost all these approaches try to identify how a specific factor, characterizing the head system, is involved into the injury and recovery procedure, oversimplifying simultaneously the other factors. This approach has the disadvantage that it cannot deal with the interference of the several parameters participating in the dynamical behaviour of the human head.

In order to improve this "monoparametric" representation of the problem, we have developed a hierarchy of models simulating in an increasing rate of accuracy the real problem [4-8]. In addition, the already existed models present solutions based rather on a "trial and error" method by matching together pieces of solutions. This approach handles

"easy" boundary conditions but cannot face more general conditions (as the neck support). Consequently the proposed models have been constructed in the basis of completeness of the involved solutions. More precisely, we have used the three-dimensional theory of dynamical elasticity not incorporating necessarily axisymmetric motions and exploited suitably the complete set of Navier eigenfunctions in order to represent, in a complete way, the elastic motion of every elastic component of the system. Every component simulated by fluid was characterized by harmonic motion represented suitably through potential functions. Considering the functions characterizing the motion of several materials as solutions of the corresponding partial differential equations and imposing on these solutions the suitable boundary conditions on discontinuity surfaces, we had to face the problem of head dynamic characteristics as a complicated boundary value problem.

Based on this approach, we have created the "sequence" of the increasingly ameliorated models by examining the dynamic characteristics of the spherical elastic skull, the spherical skull-brain system, the spherical skull-brain-neck system, the spheroidal elastic skull as well as of the bispherical elastic skull [4-8]. In all these models, the physical and geometrical constants characterising the several components of the system entered the model as parameters giving the opportunity for parametric study of the dependence of the dynamic characteristics on physical and geometrical properties.

In the sequel, we have incorporated in our study the viscoelastic properties of the skull by formatting the model of the spherical viscoelastic skull [9]. The solution procedure was much more complicated since the sought eigenfrequencies are complex numbers (the imaginary part represents the damping coefficient), fact that renders all the special functions involved difficult to be handled because of their complex argument. Overcoming this difficulty by numerical techniques of high accuracy we led to reasonable results.

In the present work we examine the elastic skull-viscoelastic brain under the assumption of spherical geometry. Matching elastic with viscoelastic solutions is a rather difficult mathematical problem as far as the numerical treatment is concerned. Focus has been given to the parametric dependence of eigenvalues and damping coefficients on the physical and geometrical characteristics of the system. The results are in accordance with the experimental results of Håkansson et al. [10]. We expect that the consideration of the viscoelastic neck will be of great importance for the determination of the real eigenfrequencies and damping coefficients of the system. An analysis based on a model which takes into account all the information obtained by our previous work on the neck support [6] is under preparation.

2. Problem Formulation

The selected model (Fig. 1) consists of an elastic sphere (1 - skull) containing a concentrically located viscoelastic material (0 - brain/cerebrospinal fluid). The skull bones are assumed to be consisted of a linear, elastic, isotropic and homogeneous material while the brain and cerebrospinal fluid are considered to be represented by a linear viscoelastic material.

The motion of the skull is described completely by the vector displacement field $\boldsymbol{u}^{(1)}(\boldsymbol{r},t)$ which satisfies the time - dependent equation of elasticity

$$\mu_1 \nabla^2 \boldsymbol{u}^{(1)}(\boldsymbol{r},t) + (\lambda_1 + \mu_1)\nabla(\nabla \cdot \boldsymbol{u}^{(1)}(\boldsymbol{r},t)) = \rho_1 \frac{\partial^2}{\partial t^2}\boldsymbol{u}^{(1)}(\boldsymbol{r},t) \qquad (1)$$

where μ_1, λ_1 are Lamè's constants, ρ_1 is the mass density, ∇ is the usual del operator, and t is the time.

The motion of the viscoelastic material V_0 is determined by the displacement field $\boldsymbol{u}^{(0)}(\boldsymbol{r},t)$ obeying the following constitutive equation

$$\tilde{\tau}(\boldsymbol{r},t) = \int_{-\infty}^{t} \left\{ \begin{array}{l} G_1(t-\tau)\dfrac{1}{2}\dfrac{\partial}{\partial\tau}\left[\nabla\boldsymbol{u}(\boldsymbol{r},t) + (\nabla\boldsymbol{u}(\boldsymbol{r},t))^T\right] + \\ \dfrac{1}{3}\left\{G_2(t-\tau) - G_1(t-\tau)\right\}\dfrac{\partial}{\partial\tau}(\nabla\cdot\boldsymbol{u}(\boldsymbol{r},t))\boldsymbol{I} \end{array} \right\} d\tau \tag{2}$$

where $\tilde{\tau}(\boldsymbol{r},t)$ is the stress tensor, $\boldsymbol{I}$ is the identity operator and $G_1(\xi)$, $G_2(\xi)$ are independent functions, having zero values for negative argument and defining the viscoelastic properties of the medium. The kinematic behaviour of the viscoelastic material is described by the equation

$$\tau_{ij,j} = \rho\ddot{u}_i, \quad i,j = 1,2,3 \tag{3}$$

where indices indicate components of the corresponding tensors while indices after the comma indicate differentiation with respect to the corresponding Cartesian coordinate.

Assuming harmonic motion of the whole system with angular frequency ω_1 and attenuation (due to viscous properties) ω_2 we apply Fourier transform analysis to the problem defining

$$\hat{u}^{(1)}(\boldsymbol{r},\omega) = \int_{-\infty}^{+\infty} \boldsymbol{u}^{(1)}(\boldsymbol{r},t)e^{-i\omega t}dt \tag{4}$$

$$\hat{u}^{(0)}(r,\omega) = \int_{-\infty}^{+\infty} \boldsymbol{u}^{(0)}(\boldsymbol{r},t)e^{-i\omega t}dt \tag{5}$$

$$\tilde{\tau}(\boldsymbol{r},\omega) = \int_{-\infty}^{+\infty} \tilde{\tau}(\boldsymbol{r},t)e^{-i\omega t}dt \tag{6}$$

and

$$g_j(\omega) = \int_0^{+\infty} G_j(t) e^{-i\omega t} dt, \quad j = 1,2 \tag{7}$$

with $\omega = \omega_1 + i\omega_2$, $i = \sqrt{-1}$.

Combining the previous equations and taking advantage of Fourier transform properties we obtain that the displacement fields $\hat{\boldsymbol{u}}^{(1)}$, $\hat{\boldsymbol{u}}^{(0)}$ satisfy the following time - independent equations of dynamic elasticity

$$\mu_1 \nabla^2 \hat{\boldsymbol{u}}^{(1)} + (\lambda_1 + \mu_1) \nabla(\nabla \cdot \hat{\boldsymbol{u}}^{(1)}) + \rho_1 \omega^2 \hat{\boldsymbol{u}}^{(1)} = \boldsymbol{0} \tag{8}$$

$$G^*(\omega) \nabla^2 \hat{\boldsymbol{u}}^{(0)} + (G^*(\omega) + \lambda^*(\omega)) \nabla(\nabla \cdot \hat{\boldsymbol{u}}^{(0)}) + \rho_0 \omega^2 \hat{\boldsymbol{u}}^{(0)} = \boldsymbol{0} \tag{9}$$

where

$$G^*(\omega) = \frac{1}{2} i\omega g_1(\omega) \tag{10}$$

$$\lambda^*(\omega) = \frac{1}{3} i\omega \left[g_2(\omega) - g_1(\omega) \right] \tag{11}$$

are the frequency functions corresponding to Lamè's constants in the case of elastic materials.

Introducing the dimensionless variables

$$\boldsymbol{r}' = \frac{\boldsymbol{r}}{\alpha}, \quad \Omega = \Omega_1 + i\Omega_2, \quad \Omega_1 = \frac{\omega_1 \alpha}{c_{p_1}}, \quad \Omega_2 = \frac{\omega_2 \alpha}{c_{p_1}}, \quad (\alpha = r_1) \tag{12}$$

equation (8) takes the following dimensionless form

$$c'^2_{s_1} \nabla'^2 \hat{\boldsymbol{u}}^{(1)}(\boldsymbol{r}') + (c'^2_{p_1} - c'^2_{s_1}) \nabla' (\nabla' \cdot \hat{\boldsymbol{u}}^{(1)}(\boldsymbol{r}')) + \Omega^2 \hat{\boldsymbol{u}}^{(1)}(\boldsymbol{r}') = 0, \quad \boldsymbol{r}' \in V_1 \tag{13}$$

where

$$\nabla' = \alpha \nabla, \quad c^2_{s_1} = \frac{\mu_1}{\rho_1}, \quad c^2_{p_1} = \frac{(\lambda_1 + 2\mu_1)}{\rho_1}, \quad c'_{s_1} = \frac{c_{s_1}}{c_{p_1}}, \quad c'_{p_1} = 1.$$

Equation (9) for the viscoelastic medium in dimensionless form is expressed as:

$$\tilde{G}_0^*(\Omega) \nabla'^2 \hat{\boldsymbol{u}}^{(0)}(\boldsymbol{r}') + (\tilde{\lambda}_0^*(\Omega) + \tilde{G}_0^*(\Omega)) \nabla' (\nabla' \cdot \hat{\boldsymbol{u}}^{(0)}(\boldsymbol{r}')) + \Omega^2 \hat{\boldsymbol{u}}^{(0)}(\boldsymbol{r}') = \boldsymbol{0}, \quad \boldsymbol{r}' \in V_0 \tag{14}$$

where

$$\tilde{G}_0^*(\Omega) = \frac{G_0^*(\Omega)}{\rho_0 c^2_{p_1}}, \quad \tilde{\lambda}_0^*(\Omega) = \frac{\lambda_0^*(\Omega)}{\rho_0 c^2_{p_1}}.$$

In equations (13,14) we have suppressed the dependence of $\hat{\boldsymbol{u}}^{(i)}(\boldsymbol{r})$ on ω for simplicity. The physical characteristics of the system enter the mathematical formulation of the problem through the boundary conditions that are described on the surfaces S_0 and S_1 (Fig. 1). The necessity of the continuity of the displacement field as well as of the traction field across S_0 leads to the conditions:

$$\hat{\boldsymbol{u}}^{(1)}(\boldsymbol{r}'_0) = \hat{\boldsymbol{u}}^{(0)}(\boldsymbol{r}'_0) \tag{15a}$$

$$\boldsymbol{T}'_1 \hat{\boldsymbol{u}}^{(1)}(\boldsymbol{r}'_0) = \boldsymbol{T}'_0 \hat{\boldsymbol{u}}^{(0)}(\boldsymbol{r}'_0) \tag{15b}$$

where

$$\boldsymbol{T}'_i = 2\mu'_i \circ\hat{\boldsymbol{r}}\nabla' + \lambda'_i \circ\hat{\boldsymbol{r}}(\nabla' \cdot) + \mu'_i \circ\hat{\boldsymbol{r}} \times \nabla' \times \tag{16}$$

denotes the surface traction operator in the i-medium, $\hat{\boldsymbol{r}}$ is the outer unit normal vector on S_0, and

$$\mu'_i = \begin{cases} 1, & i = 1 \\ \dfrac{G_0^*(\omega)}{\mu_1}, & i = 0 \end{cases}, \lambda'_i = \begin{cases} \dfrac{\lambda_1}{\mu_1}, & i = 1 \\ \dfrac{\lambda_0^*(\omega)}{\mu_1}, & i = 0 \end{cases}. \tag{17}$$

Since the outer surface of the skull, S_1, is stress free, we lead to the condition:

$$\boldsymbol{T}'_1 \hat{\boldsymbol{u}}^{(1)}(\boldsymbol{r}'_1) = 0. \tag{18}$$

We note that the problem described by the equations (13) and (14) and the boundary conditions (15) and (18) is a well - posed mathematical problem.

3. Problem Solution

Adopting the methodology followed by Charalambopoulos et al. [4], we expand the displacement fields in the regions 0 and 1 in terms of the Navier eigenfunctions [11], which constitute a complete set of vector functions in the space of square integrable

functions in the region occupied by the system under investigation. More precisely, the displacement field in the 1 - region has the full expansion

$$\hat{\boldsymbol{u}}^{(1)}(\boldsymbol{r}) = \sum_{n=0}^{\infty} \sum_{m=-n}^{n} \sum_{l=1}^{2} \left\{ \alpha_{n,1}^{m,l} \boldsymbol{L}_{n,1}^{m,l}(\boldsymbol{r}) + \beta_{n,1}^{m,l} \boldsymbol{M}_{n,1}^{m,l}(\boldsymbol{r}) + \gamma_{n,1}^{m,l} \boldsymbol{N}_{n,1}^{m,l}(\boldsymbol{r}) \right\}, \quad \boldsymbol{r} \in V_1 \tag{19a}$$

and for the 0 - region

$$\hat{\boldsymbol{u}}^{(0)}(\boldsymbol{r}) = \sum_{n=0}^{\infty} \sum_{m=-n}^{n} \left\{ \alpha_{n,o}^{m,1} \boldsymbol{L}_{n,0}^{m,1}(\boldsymbol{r}) + \beta_{n,0}^{m,1} \boldsymbol{M}_{n,0}^{m,1}(\boldsymbol{r}) + \gamma_{n,0}^{m,1} \boldsymbol{N}_{n,0}^{m,1}(\boldsymbol{r}) \right\}, \quad \boldsymbol{r} \in V_0 \tag{19b}$$

where

$$\begin{aligned}
\boldsymbol{L}_n^{m,l}(\boldsymbol{r}') &= \dot{g}_n^l(k'_p r') \boldsymbol{P}_n^m(\hat{\boldsymbol{r}}) + \sqrt{n(n+1)} \frac{g_n^l(k'_p r')}{k'_p r'} \boldsymbol{B}_n^m(\hat{\boldsymbol{r}}) \\
\boldsymbol{M}_n^{m,l}(\boldsymbol{r}') &= \sqrt{n(n+1)} g_n^l(k'_s r') \boldsymbol{C}_n^m(\hat{\boldsymbol{r}}) \\
\boldsymbol{N}_n^{m,l}(\boldsymbol{r}') &= n(n+1) \frac{g_n^l(k'_s r')}{k'_s r'} \boldsymbol{P}_n^m(\hat{\boldsymbol{r}}) + \sqrt{n(n+1)} \left\{ \dot{g}_n^l(k'_s r') + \frac{g_n^l(k'_s r')}{k'_s r'} \right\} \boldsymbol{B}_n^m(\hat{\boldsymbol{r}}),
\end{aligned} \tag{20}$$

$$k'_{p_i} = \begin{cases} \Omega, & i = 1 \\ \dfrac{\Omega}{(\tilde{\lambda}_0^*(\Omega) + 2\tilde{G}_0^*(\Omega))^{1/2}}, & i = 0 \end{cases} \tag{21}$$

$$k'_{s_i} = \begin{cases} \dfrac{\Omega}{c'_{s_1}}, & i = 1 \\ \dfrac{\Omega}{(\tilde{G}_0^*(\Omega))^{1/2}}, & i = 0 \end{cases} \tag{22}$$

and $g_n^1(z)$, $g_n^2(z)$ represent the spherical Bessel functions of the first, $j_n(z)$ and second kind $y_n(z)$, respectively.

The functions $\boldsymbol{P}_n^m(\hat{\boldsymbol{r}})$, $\boldsymbol{B}_n^m(\hat{\boldsymbol{r}})$ and $\boldsymbol{C}_n^m(\hat{\boldsymbol{r}})$ defined on the unit sphere, are the vector spherical harmonics introduced by Hansen [11] and in spherical polar coordinates (r,ϑ,φ) are given as follows

$$\boldsymbol{P}_n^m(\hat{\boldsymbol{r}}) = \hat{\boldsymbol{r}} Y_n^m(\hat{\boldsymbol{r}})$$

$$\boldsymbol{B}_n^m(\hat{r}) = \frac{1}{\sqrt{n(n+1)}}\left\{\hat{\vartheta}\frac{\partial}{\partial\vartheta} + \hat{\varphi}\frac{1}{\sin\vartheta}\frac{\partial}{\partial\varphi}\right\}Y_n^m(\hat{r}) \tag{23}$$

$$\boldsymbol{C}_n^m(\hat{r}) = \frac{1}{\sqrt{n(n+1)}}\left\{\hat{\vartheta}\frac{1}{\sin\vartheta}\frac{\partial}{\partial\varphi} - \hat{\varphi}\frac{\partial}{\partial\vartheta}\right\}Y_n^m(\hat{r}),$$

where $\hat{\vartheta}$ and $\hat{\varphi}$ are the unit vectors in ϑ and φ - directions, respectively, $Y_n^m(\hat{r}) = P_n^m(\cos\vartheta)e^{im\varphi}$ are the spherical harmonics and $P_n^m(\cos\vartheta)$ are the well - known Legendre functions.

As it is obvious the problem of the determination of $\boldsymbol{u}^{(0)}$ and $\boldsymbol{u}^{(1)}$ is transferred to the determination of the coefficients in the expansions (19a) and (19b) in terms of the Navier eigenfunctions, since the expressions (19a) and (19b) satisfy Navier's equations. We ask these expressions to obey the boundary conditions (15a) and (15b).

The presence of the surface stress operator in the boundary conditions requires the knowledge of the way this operator acts on the Navier eigenfunctions. Tedious and extended manipulations lead to the following relations

$$\boldsymbol{T}_i \boldsymbol{L}_{n,i}^{m,l}(r') = -\begin{bmatrix} \frac{4\mu'_i}{r'} \dot{g}_n^l(k'_{p_i} r') + 2\mu'_i k'_{p_i} \left(1 - \frac{n(n+1)}{k'^2_{p_i} r'^2}\right) g_n^l(k'_{p_i} r') + \\ \lambda'_i k'_{p_i} g_n^l(k'_{p_i} r') \end{bmatrix} \times \boldsymbol{P}_n^m(r') \\ +2\mu'_i \sqrt{n(n+1)} \left[\frac{\dot{g}_n^l(k'_{p_i} r')}{r'} - \frac{g_n^l(k'_{p_i} r')}{k'_{p_i} r'^2} \right] \boldsymbol{B}_n^m(\hat{\boldsymbol{r}}) \tag{24a}$$

$$\boldsymbol{T}_i \boldsymbol{M}_{n,i}^{m,l}(r') = \mu'_i \sqrt{n(n+1)} \left[k'_{s_i} \dot{g}_n^l(k'_{s_i} r') - \frac{1}{r'} g_n^l(k'_{s_i} r') \right] \boldsymbol{C}_n^m(\hat{\boldsymbol{r}}) \tag{24b}$$

$$\boldsymbol{T}_i \boldsymbol{N}_{n,i}^{m,l}(r') = 2\mu'_i n(n+1) \left[\frac{\dot{g}_n^l(k'_{s_i} r')}{r'} - \frac{g_n^l(k'_{s_i} r')}{k'_{s_i} r'^2} \right] \boldsymbol{P}_n^m(\hat{\boldsymbol{r}}) \\ +\mu'_i n(n+1) \left[-\frac{2\dot{g}_n^l(k'_{s_i} r')}{r'} - k'_{s_i} g_n^l(k'_{s_i} r') + 2\frac{n(n+1)}{k'_{s_i} r'^2} g_n^l(k'_{s_i} r') \right] \boldsymbol{B}_n^m(\hat{\boldsymbol{r}}) \tag{24c}$$

Inserting (19a) and (19b) in the boundary conditions (15a) and (15b), using the expressions (24a, b, c) and taking the advantage of the independence of the Navier eigenfunctions we conclude that for every specific pair of integers (n,m) (with $|m| \le n$) the nine coefficients involved in the expansions (19a) and (19b), satisfy a linear homogeneous system with nine equations of the form

$$\boldsymbol{D}_n^m \boldsymbol{x}_n^m = \boldsymbol{0} \tag{25}$$

where

$$\boldsymbol{x}_n^m = \left[\alpha_{n,1}^{m,1}, \alpha_{n,1}^{m,2}, \beta_{n,1}^{m,1}, \beta_{n,1}^{m,2}, \gamma_{n,1}^{m,1}, \gamma_{n,1}^{m,2}, \alpha_{n,0}^{m,1}, \beta_{n,0}^{m,1}, \gamma_{n,0}^{m,1} \right]^T$$

and the elements of matrix $\boldsymbol{D}_n^m$ are given in the Appendix.

The existence of nontrivial solutions of (25) imposes the condition

$$\det\left(\boldsymbol{D}_n^m(\Omega_1,\Omega_2)\right)=0 \tag{26}$$

which is the characteristic equation from which we obtain the eigenfrequency and damping coefficients $\Omega_1{}^m$, $\Omega_2{}^m$, respectively for $m=1,2,3,.....$

4. Numerical Solution

The equation (25) is solved numerically in order to obtain the solution $\Omega^m=\Omega_1^m+i\Omega_2^m$ using a complex LU - decomposition routine. The computation of spherical Bessel and Neumann functions along with their derivatives for complex arguments [12] makes the computation time intensive. The computed terms are shown in the Appendix.

Finally with the use of a matrix determinant computation routine we lead to

$$\mathrm{Re}\left[\det\left(\boldsymbol{D}_n^m(\Omega_1,\Omega_2)\right)\right]+i\,\mathrm{Im}\left[\det\left(\boldsymbol{D}_n^m(\Omega_1,\Omega_2)\right)\right]=0 \tag{27}$$

or

$$\mathrm{Re}\left[\det\left(\boldsymbol{D}_n^m(\Omega_1,\Omega_2)\right)\right]=0,\ \text{and}\ \mathrm{Im}\left[\det\left(D_n^m(\Omega_1,\Omega_2)\right)\right]=0. \tag{28}$$

The results obtained correspond to material properties analogous to those proposed elsewhere.

For the human skull [13]

$$E = 1.379x10^9\ N/m^2,\ \ \nu = 0.25,\ \ \rho = 2.1326x10^3\ Kg/m^3.$$

For the viscoelastic brain we ignore the directional properties and the material is considered isotropic. We note that the properties of the grey matter show directional preference and differ from those of white matter. However, the differences are quite small so that average values for white and grey matter in all directions are used [14].

The viscoelastic properties of brain have been measured by Shuck and Advani [14] who have considered their dependence on eigenfrequency ω_1 . In their analysis the measured experimental data correspond to a frequency spectrum from 0 to 350 Hz. It is well known that the experimental resonance frequencies of the human head fall in the region 0 - 7.5 KHz, and the measured properties of brain must be extrapolated.

In our analysis we use the extrapolation presented in Ref. 15 which uses a linear extrapolation for $G_1(\omega_1)$ and $G_2(\omega_1)$ is given by

$$G_2(\omega_1) = \frac{2\omega_1}{\pi}\left[\int_0^{100} \frac{G_1(\omega_1) - G_1(0)}{\alpha^2 - \omega^2} d\alpha + \int_{100}^{\omega_1} \frac{G_1(\omega_1) - G_1(0)}{\alpha^2 - \omega^2} d\alpha + \text{const.}\right], \qquad (29)$$

where the const. term is computed on the basis of the difference $G_2(\omega_1)_{computed} - G_2(\omega_1)_{\exp.}$ for the frequency region 100 - 350 Hz. The properties used are shown in Table 1.

The geometrical parameteres are averages of those used in the experimental work of Ref. 10, that is:

$$r_1 = 0.0854m,\ r_0 \in [0.040 - 0.0794m].$$

The solution of the system of equations (28) is obtained by a bisection grid method on the (Ω_1, Ω_2) - plane and identification of those squares where are zero - crossings of the real and imaginary parts of the determinant curves. This is analytically presented in Ref. 9. The accuracy of our computation is 10^{-6} in each direction.

The solution obtained for the system under consideration is presented in Fig. 2 for $n = 1,2,...,8$. In the figure the crossing of curves indicates complex solution, $\Omega = \Omega_1 + i\Omega_2$.

The solution $\Omega = \Omega_1 + i\Omega_2$, as well as, the dimensional one $\omega = \omega_1 + i\omega_2$ is presented in Table 2. In the same table the results of our FF - Model [5], in which the brain is modelled as an inviscid, irrotational fluid, are given. The comparison shows that the viscoelastic brain model gives eigengrequencies which are close to the ones predicted by the FF-Model and for the computation of those characteristics this model is sufficient and complex arithmetic can be avoided. However, the model under discussion predicts the damping coefficients of the system.

The same comparison for a smaller inner skull radius is shown ($r_0 = 0.040m$) in Table 3. Again the eigenfrequency coefficients are close to those predicted by the FF-Model and the calculated damping coefficients much smaller than those presented in Table 3.

A comparison of the results obtained, using the above described method, with experimental ones [10] is given in Table 4. It is noted that in the comparison the first two modes are not given since we know that the prediction of the first two eigenfrequencies can be done only by models which include neck support [6]. The results are in excellent agreement with the measured eigenfrequency coefficients and most of the predicted damping coefficients are within the order of magnitude of the measured ones but they do not fall in the region of experimental ones. However, two of them (7th and 8th) are predicted within the bounds of the experimental method used. This implies that the viscoelasticity of the skull, as well as, the viscoelasticity of the neck support [16] must be included, work which is under preparation.

It is noted that in our computations ω_2 (or Ω_2) corresponds to 1 - 5 % of ω_1 (or Ω_1) which compares with 3 - 10 % found in the experimental data. Other researchers [1] could not predict those small damping coefficients and in their analysis the damping

coefficients found, Ω_2, are much bigger than eigenfrequency coefficients Ω_1. This is due to the inaccurate computation of the special functions involved in the computations.

The effect of inner radius on the eigengrequency and damping spectra is shown in Table 5 and graphically in Fig. 3. The effect of brain density (without change of other characteristics) is shown in Table 6 and graphically in Fig. 4.

5. Concluding Remarks

In this work we presented a mathematical analysis for the study of the eigenfrequencies of the human skull - brain system in the framework of the three-dimensional theory of linear viscoelasticity. The geometry of the physical system considered has been modelled by the FF - Model where the outer hollow elastic sphere represents the skull and the inner space is supposed to be filled with a viscoelastic material corresponding to the brain / cerebrospinal fluid.

The proposed analysis was used to calculate the eigenfrequencies of the simulated system. We note that the results obtained are in excellent agreement with the measured eigenfrequency coefficients and most of the predicted damping coefficients are within the order of magnitude of the measured ones but they do not fall in the region of experimental ones (two of them were found within the bounds of the measured ones). We believe that the discrepancy between the results obtained and those from the experiment exists because we have not taken into account the viscoelastic properties of the skull as well as the neck support. The analysis which avoids the drawbacks of the present work is under preparation.

ACKNOWLEDGEMENT

The present work forms part of the project "New Systems for Early Medical Diagnosis and Biotechnological Applications" which is supported by the Greek General Secretariat for Research and Technology through the EU funded R&D Program EPET II.

REFERENCES

[1] Misra J.C. and Chakravarty S., A Free - Vibration Analysis for the Human Cranial System, J. Biomechanics 15 635-645 (1982).

[2] Guarino J.C. and Elger D.F., Modal Analysis of a Fluid - Filled Elastic Shell Containing an Elastic Sphere, J. of Sound and Vibration 156 461-479 (1992).

[3] Advani S.H., and Owings R.P., Structural Modelling of Human Head, J. of the Engineering Mechanics Division, American Society of Civil Engineers 101 257-266 (1975).

[4] Charalambopoulos A., Dassios G., Fotiadis D.I., Kostopoulos V., Massalas C.V., On the Dynamic Characteristics of the Human Skull, International Journal of Engineering Science, 34(12) 1339-1348 (1996)

[5] Charalambopoulos A., Dassios G., Fotiadis D.I., Massalas C.V., The Dynamic Characteristics of the Human Skull - Brain System, Mathematical and Computer Modelling, accepted (1996).

[6] Charalambopoulos A., Dassios G., Fotiadis D.I., Massalas C.V., The dynamic Characteristics of the Human Head-Neck System, International Journal of Engineering Science, accepted (1996).

[7] Charalambopoulos A., Fotiadis D.I., Massalas C.V., The Effect of Geometry on the Dynamic Characteristics of the Human Skull, International Journal of Engineering Science, accepted (1996).

[8] Charalambopoulos A., Fotiadis D.I., Massalas C.V., Frequency Spectrum of the Bispherical Hollow System: The Case of the Nonuniform Thickness Human Skull, Acta Mechanica , accepted (1997).

[9] Charalambopoulos A., Fotiadis D.I., Massalas C.V., Free Vibrations of the Human Viscoelastic Skull, International Journal of Engineering Science, accepted (1997).

[10] HåkansonB., Brandt A. and Carlsson P., J. Acoust. Soc. Am. 95(3) 1474 (1994).

[11] Hansen W.W., Phys. Rev. 47 139 (1935).

[12] Zhang S. and Jin J., Computation of Special Functions, Wiley - Interscience (1996).

[13] McElhaney J.H., Fogle J.L., Melvin J.W., Haynes R.R., Roberts V.L. and Alem N.M., Mechanical Properties of Cranial Bone, J. of Biomechanics, 3 495-511 (1970).

[14] Schuck L.Z., Advani S.H., Rheological Response of Human Brain Tissue in Shear, Transactions of the ASME, Journal of Basic Engineering, 905-911 (1972).

[15] Hickling R. and Wenner M.L., Mathematical Model of a Head Subjected to an Axisymmetric Impact, J. of Biomechanics, 6 115-132 (1973).

[16] Landkoff B. and Goldsmith W., Impact of a Head - Neck Structure, J. of Biomechanics, 9 141-151 (1976).

APPENDIX

$$d_{1,1} = A^1_{n,1}(r'_1),\ d_{1,2} = A^2_{n,1}(r'_1),\ d_{1,5} = D^1_{n,1}(r'_1),\ d_{1,6} = D^2_{n,1}(r'_1),\ d_{2,3} = C^1_{n,1}(r'_1),$$

$$d_{2,4} = C^2_{n,1}(r'_1),\ d_{3,1} = B^1_{n,1}(r'_1),\ d_{3,2} = B^2_{n,1}(r'_1),\ d_{4,1} = \dot{j}_n(\Omega r'_0),\ d_{4,2} = \dot{y}_n(\Omega r'_0),$$

$$d_{4,5} = n(n+1) j_n(\Omega(2+\lambda'_1)^{1/2} r'_0) \frac{1}{\Omega(2+\lambda'_1)^{1/2} r'_0},$$

$$d_{4,6} = n(n+1) y_n(\Omega(2+\lambda'_1)^{1/2} r'_0) \frac{1}{\Omega(2+\lambda'_1)^{1/2} r'_0},$$

$$d_{4,7} = -j_n(\xi_{p,10}\Omega r'_0),$$

$$d_{4,9} = -n(n+1) j_n\left(\xi_{p,10}\Omega\left(2+\frac{\lambda'_0}{\mu'_0}\right)^{1/2} r'_0\right) \frac{1}{\xi_{p,10}\Omega\left(2+\frac{\lambda'_0}{\mu'_0}\right)^{1/2} r'_0},$$

$$d_{5,3} = j_n\left((2+\lambda'_1)^{1/2}\Omega r'_0\right),\ d_{5,4} = y_n\left((2+\lambda'_1)^{1/2}\Omega r'_0\right),\ d_{5,8} = -j_n\left(\left(2+\frac{\lambda'_0}{\mu'_0}\right)^{1/2}\Omega r'_0\right),$$

$$d_{6,1} = \frac{j_n(\Omega r'_0)}{\Omega r'_0},\ d_{6,2} = \frac{y_n(\Omega r'_0)}{\Omega r'_0},\ d_{6,5} = \dot{j}_n\left((2+\lambda'_1)^{1/2}\Omega r'_0\right) + \frac{j_n\left((2+\lambda'_1)^{1/2}\Omega r'_0\right)}{(2+\lambda'_1)^{1/2}\Omega r'_0},$$

$$d_{6,6} = \dot{y}_n\left((2+\lambda'_1)^{1/2}\Omega r'_0\right) + \frac{y_n\left((2+\lambda'_1)^{1/2}\Omega r'_0\right)}{(2+\lambda'_1)^{1/2}\Omega r'_0},\ d_{6,7} = -\frac{j_n(\xi_{p,10}\Omega r'_0)}{\xi_{p,10}\Omega r'_0}$$

$$d_{6,9} = -\left[\dot{j}_n\left(\left(2+\frac{\lambda'_0}{\mu'_0}\right)^{1/2}\xi_{p,10}\Omega\right) + \frac{j_n\left(\left(2+\frac{\lambda'_0}{\mu'_0}\right)^{1/2}\xi_{p,10}\Omega\right)}{\left(2+\frac{\lambda'_0}{\mu'_0}\right)^{1/2}\xi_{p,10}\Omega}\right],$$

$$d_{7,1} = A^1_{n,1}(r'_0),\ d_{7,2} = A^2_{n,1}(r'_0),\ d_{7,5} = D^1_{n,1}(r'_0),\ d_{7,6} = D^2_{n,1}(r'_0),\ d_{7,7} = -A^1_{n,0}(r'_0),$$

$$d_{7,9} = -D^1_{n,0}(r'_0),\ d_{8,3} = C^1_{n,1}(r'_0),\ d_{8,4} = C^2_{n,1}(r'_0),\ d_{8,8} = -C^1_{n,0}(r'_0),\ d_{9,1} = B^1_{n,1}(r'_0),$$

$$d_{9,2} = B^2_{n,1}(r'_0),\ d_{9,5} = E^1_{n,1}(r'_0),\ d_{9,6} = E^2_{n,1}(r'_0),\ d_{9,7} = -B^1_{n,0}(r'_0),\ d_{9,9} = -E^1_{n,0}(r'_0)$$

where

$$A^l_{n,i}(r') = -\begin{bmatrix} \frac{4\mu'_i}{r'}\dot{g}^l_n(\xi_{p,1i}\Omega r') + 2\mu'_i\xi_{p,1i}\Omega \\ \left(1-\frac{n(n+1)}{\xi^2_{p,1i}\Omega^2 r'^2}\right)g^l_n(\xi_{p,1i}\Omega r') + \lambda'_i\xi_{p,1i}\Omega g^l_n(\xi_{p,1i}\Omega r') \end{bmatrix},$$

$$B^l_{n,i}(r') = 2\mu'_i\sqrt{n(n+1)}\left[\frac{1}{r'}\dot{g}^l_n(\xi_{p,1i}\Omega r') - \frac{g^l_n(\xi_{p,1i}\Omega r')}{\xi_{p,1i}\Omega r'^2}\right],$$

$$C^l_{n,i}(r') = \mu'_i\sqrt{n(n+1)}\begin{bmatrix} \left(2+\frac{\lambda'_i}{\mu'_i}\right)^{1/2}\xi_{p,1i}\Omega\dot{g}^l_n\left(\left(2+\frac{\lambda'_i}{\mu'_i}\right)^{1/2}\xi_{p,1i}\Omega r'\right) \\ -\frac{1}{r'}\left(2+\frac{\lambda'_i}{\mu'_i}\right)^{1/2}\xi_{p,1i}\Omega r' \end{bmatrix},$$

$$D^l_{n,i}(r') = 2\mu'_i n(n+1)\begin{bmatrix} \frac{1}{r'}\dot{g}^l_n\left(\left(2+\frac{\lambda'_i}{\mu'_i}\right)^{1/2}\xi_{p,1i}\Omega r'\right) \\ -\frac{1}{\left(2+\frac{\lambda'_i}{\mu'_i}\right)^{1/2}\xi_{p,1i}\Omega r'^2}g^l_n\left(\left(2+\frac{\lambda'_i}{\mu'_i}\right)^{1/2}\xi_{p,1i}\Omega r'\right) \end{bmatrix},$$

$$E^l_{n,i}(r') = \mu'_i n(n+1)\begin{bmatrix} -2\frac{1}{r'}\dot{g}^l_n\left(\left(2+\frac{\lambda'_i}{\mu'_i}\right)^{1/2}\xi_{p,1i}\Omega r'\right) \\ -\left(2+\frac{\lambda'_i}{\mu'_i}\right)^{1/2}\xi_{p,1i}\Omega g^l_n\left(\left(2+\frac{\lambda'_i}{\mu'_i}\right)^{1/2}\xi_{p,1i}\Omega r'\right) \\ +\frac{2(n(n+1)-1)}{\left(2+\frac{\lambda'_i}{\mu'_i}\right)^{1/2}\xi_{p,1i}\Omega r'^2}g^l_n\left(\left(2+\frac{\lambda'_i}{\mu'_i}\right)^{1/2}\xi_{p,1i}\Omega r'\right) \end{bmatrix},$$

and

$$\xi_{p,1i} = \begin{cases} 1 & i=1 \\ \left[\frac{\lambda_1+2\mu_1}{\lambda^*_0(\omega_1)+2G^*_0(\omega_1)}\right]^{1/2}\left(\frac{\rho_0}{\rho_1}\right)^{1/2} & i=0 \end{cases}$$

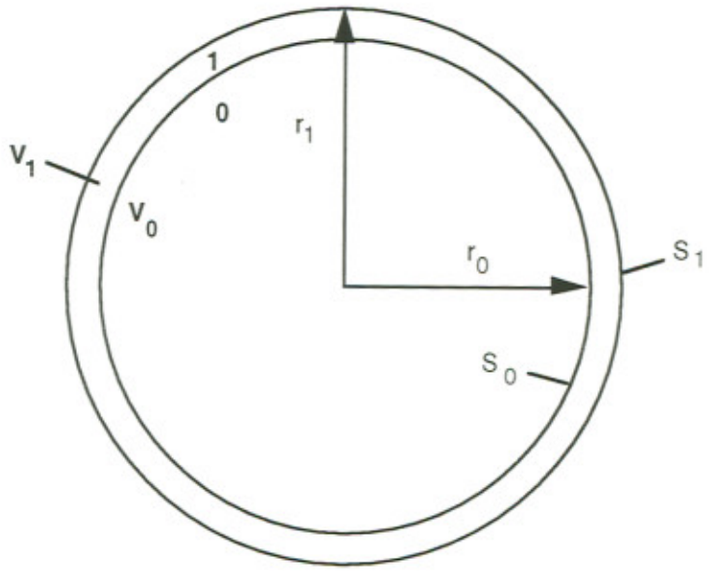

Figure 1: Problem Geometry

Figure 2: Solution of (2:) in the complex plane (Ω_1, Ω_2) for $r_0 = 0.010m$, $r_1 = 0.0854m$ and $n = 1,...,4$.

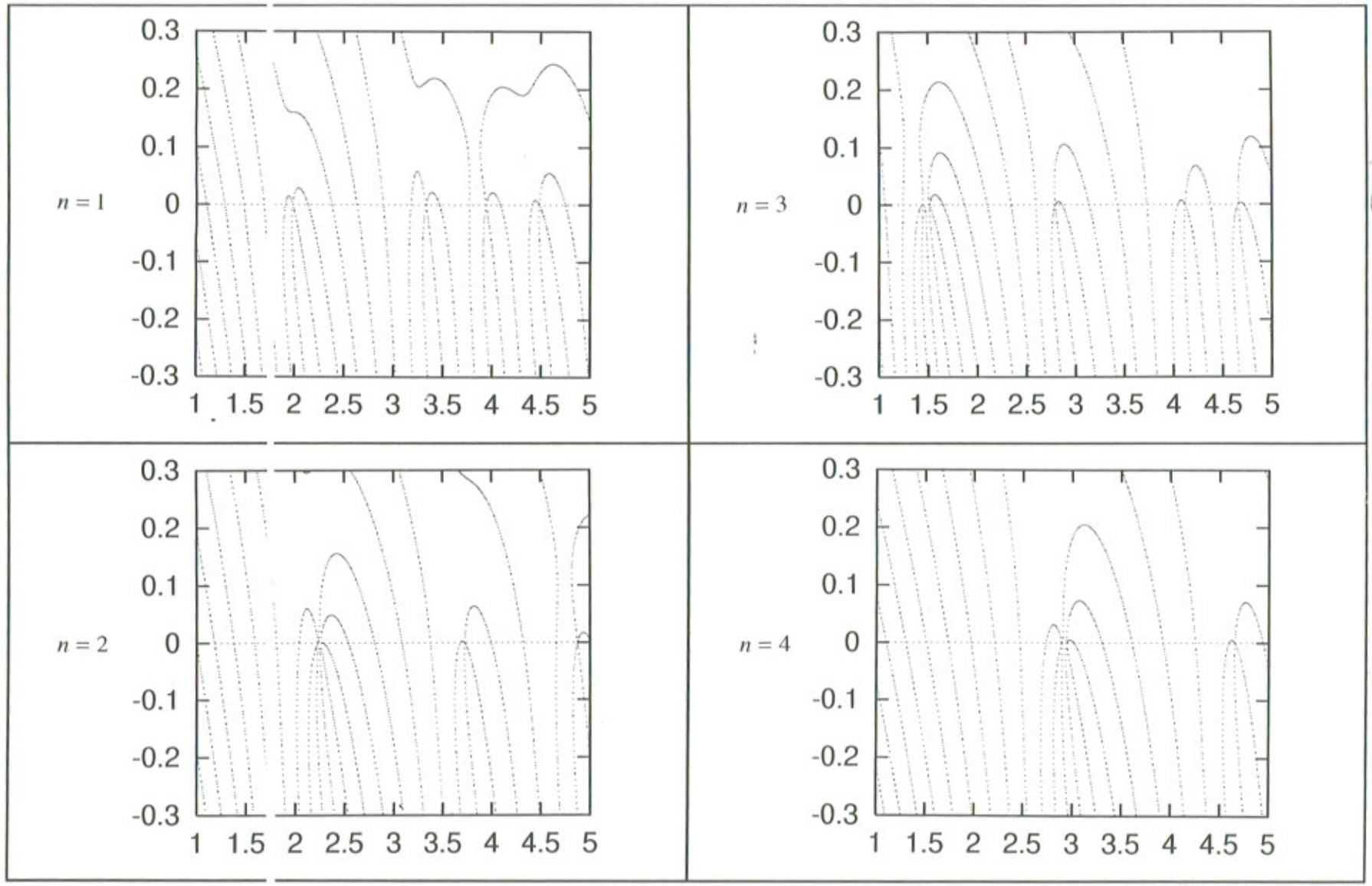

Table 1: Variation of brain properties with ω_1.

$f = \frac{\omega}{2\pi}$	ω	$G_1\ (N/m^2)$	$G_2\ (N/m^2)$	$\lambda_1(N/m^2)$	$\lambda_2(N/m^2)$
5	31.42	0.76×10^4	0.276×10^4	2.1030×10^9	-0.184×10^4
35	219.91	1.17×10^4	0.517×10^4	2.1030×10^9	-0.345×10^4
65	408.41	1.72×10^4	0.965×10^4	2.1030×10^9	-0.643×10^4
95	596.90	2.00×10^4	1.57×10^4	2.1030×10^9	-1.047×10^4
125	785.40	2.28×10^4	2.28×10^4	2.1030×10^9	-1.520×10^4
175	1099.56	2.62×10^4	3.45×10^4	2.1030×10^9	-2.300×10^4
255	1602.21	3.04×10^4	5.38×10^4	2.1030×10^9	-3.587×10^4
350	2199.11	3.39×10^4	8.14×10^4	2.1030×10^9	-5.427×10^4
674	4237.00	4.62×10^4	8.40×10^4	2.1030×10^9	-5.601×10^4
999	6274.89	5.84×10^4	12.10×10^4	2.1030×10^9	-8.067×10^4
1323	8312.84	7.06×10^4	15.73×10^4	2.1030×10^9	-10.483×10^4
1647	10350.73	8.28×10^4	19.29×10^4	2.1030×10^9	-12.863×10^4
1972	12388.62	9.50×10^4	22.80×10^4	2.1030×10^9	-15.199×10^4

Table 2: Eigenfrequency and attenuation spectra for $r_0 = 0.0794m$.

FF [5]		Viscoelastic Brain			
Ω	ω	Ω_1	ω_1	Ω_2	ω_2
0.3993	1466.504	0.39843 (n=2)	1463.308	0.16872×10^{-2}	6.196
0.5172	1899.513	0.51540 (n=3)	1892.902	0.34851×10^{-2}	12.799
0.6146	2257.233	0.61220 (n=4)	2248.419	0.49866×10^{-2}	18.314
0.7237	2657.923	0.72092 (n=5)	2647.713	0.63062×10^{-2}	23.161
0.8614	3163.652	0.85809 (n=6)	3151.495	0.75336×10^{-2}	27.669
1.0348	3800.496	1.03137 (n=7)	3787.898	0.87177×10^{-2}	32.017
1.1575	4251.134	1.13251 (n=1)	4159.354	0.35611×10^{-1}	130.788
1.1955	4390.696	1.17618 (n=2)	4319.740	0.26437×10^{-1}	97.095
1.2467	4578.738	1.24305 (n=8)	4565.333	0.98743×10^{-2}	36.265

Table 3: Eigenfrequency and attenuation spectra for $r_0 = 0.040m$.

FF [5]		Viscoelastic Brain			
Ω	ω	Ω_1	ω_1	Ω_2	ω_2
1.1154	4096.51	1.1153 (n=2)	4096.37	0.16174×10^{-3}	0.59402
1.4147	5195.75	1.41439 (n=2)	5194.61	0.40955×10^{-3}	1.50415
1.8301	6721.38	1.83012 (n=3)	6721.46	0.31189×10^{-3}	1.14547
1.8921	6949.09	1.88872 (n=4)	6939.68	0.51831×10^{-2}	19.03590
2.2106	8118.84	2.21032 (n=3)	8117.81	0.31250×10^{-3}	1.14771
2.5705	9440.64	2.57046 (n=4)	9440.49	0.38208×10^{-3}	1.40326
2.6818	9849.41	2.68058 (n=2)	9844.93	0.18622×10^{-2}	6.83928
2.9295	10759.13	2.92934 (n=4)	10758.55	0.19531×10^{-3}	0.71732
3.1913	11720.64	3.17475 (n=1)	11659.86	0.25924×10^{-1}	95.21072

Table 4: Comparison with experimental measurements [10].

Experiment * ω_1 [10]	ω_1	Experiment * ω_2 [10]	ω_2
853 - 1091		49.6 - 123.4	
1082 - 1378		49.2 - 127.9	
1373 - 1691	1463.308	33.7 - 183.8	6.196
1616 - 1954	1892.902	51.8 - 137.4	12.799
1859 - 2293	2248.419	93.4 - 213.8	18.314
2084 - 2490	2647.713	123.5 - 201.3	23.161
2260 - 2876	3151.495	95.0 - 161.8	27.669
2510 - 3288	3787.898	72.5 - 136.3	32.017
3213 - 3967	4159.354	87.8 - 159.4	130.788
3558 - 4644	4319.740	89.8 - 226.2	97.095
4197 - 5389	4565.333	135.3 - 258.4	36.265

* *It is noted that in [10] the neck is included*

Table 5: Variation of eigenfrequency and damping coefficients spectra with inner radius.

$r_0/r_1 = 0.117$		$r_0/r_1 = 0.468$		$r_0/r_1 = 0.703$		$r_0/r_1 = 0.930$	
ω_1	ω_2	ω_1	ω_2	ω_1	ω_2	ω_1	ω_2
5303.32	0.000	4096.37	0.594	2812.98	1.867	1463.308	6.196
5555.56	0.018	5194.61	1.504	4232.44	3.292	1892.902	12.799
7272.40	0.004	6721.46	1.145	4847.65	11.970	2248.419	18.314
8194.79	0.000	6939.68	19.036	5505.39	49.185	2647.713	23.161
8301.04	0.002	8117.81	1.148	6003.26	4.434	3151.495	27.669
10257.89	0.047	9440.49	1.403	7658.65	12.136	3787.898	32.017
10621.74	0.000	9844.93	6.839	9298.98	55.601	4159.354	130.788
10802.77	0.000	10758.55	0.717	10261.01	15.144	4319.740	97.095
12227.03	0.518	11659.86	95.211	11206.80	49.185	4565.333	36.265

Figure 3: Variation of eigenfrequency and damping coefficients spectra with inner radius (A: eigenfrequency coefficients, B: damping coefficients).

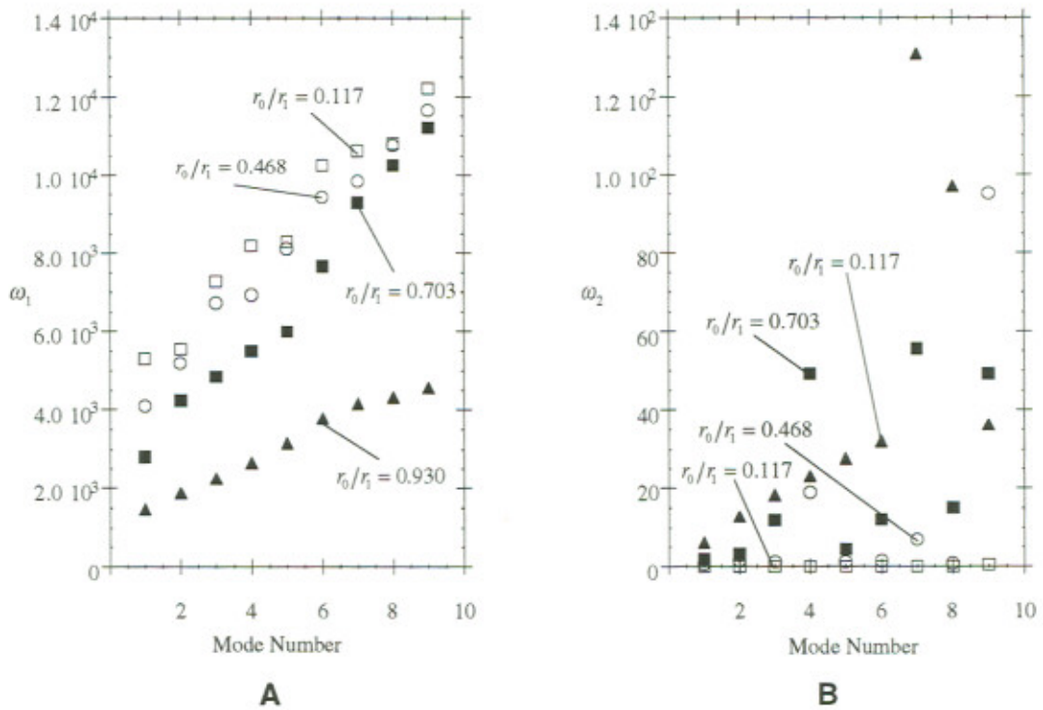

Table 5: Variation of eigenfrequency and damping coefficients spectra with brain density.

$\rho_0/\rho_1 = 0.422$		$\rho_0/\rho_1 = 0.469$		$\rho_0/\rho_1 = 0.516$	
ω_1	ω_2	ω_1	ω_2	ω_1	ω_2
1516.56	6.402	1463.308	6.196	1415.29	6.001
1956.04	13.180	1892.902	12.799	1835.50	12.429
2316.53	18.740	2248.419	18.314	2185.95	17.866
2720.79	23.627	2647.713	23.161	2580.17	22.688
3230.89	28.108	3151.495	27.669	3077.09	27.207
3876.19	32.411	3787.898	32.017	3705.34	31.587
4214.96	128.085	4159.354	130.788	4111.83	133.443
4323.34	92.104	4319.740	97.095	4316.32	101.836
4663.87	35.595	4565.333	36.265	4472.67	35.884

Figure 4: Variation of eigenfrequency and damping coefficients spectra with brain density (A: eigenfrequency coefficients, B: damping coefficients).